Recent Advancements in Lorentz Force Eddy Current Testing

Reinhard SCHMIDT [1], Konstantin WEISE [1], Matthias CARLSTEDT [1], Marek ZIOLKOWSKI [1], Hartmut BRAUER [1], Stephan GORGES [1]
[1] Technische Universität Ilmenau, Ilmenau, Germany

Contact e-mail: hartmut.brauer@tu-ilmenau.de

Abstract. We present advancements in the recently introduced Lorentz force eddy current testing (LET) which is a based on the relative motion between a permanent magnet and the electrically conducting object under test. We developed a new cylindrical magnetic Halbach structure which is designed to focus the magnetic field below the structure. A multi-objective optimization was implemented to maximize the defect response for a given defect scenario of interest. Secondly, we investigated the uncertainties in our experimental setup by means of an analysis of variance based on the generalized polynomial chaos expansion of the probability density functions of several input parameters. Finally, a defect depth study using a quasi-infinite crack was performed in order to determine a detection limit for LET.

1. Introduction

In classical eddy current testing (ECT) an alternating current is driving a coil inducing a magnetic field whose variations are analyzed in order to detect anomalies in conductivity by means of a secondary coil for example. In contrast to ECT in motion induced eddy current testing (MECT) the induced eddy currents are generated by a relative movement of a stationary magnetic field source to an electrically conducting object under test. In the recent years a variety of methods in the field of MECT can be observed. Ramos et al. used DC coils as moving stationary magnetic field measuring the magnetic field by GMR sensors [1]. Tan et al. proposed a rotating diametral magnetized permanent magnet evaluating disturbances in the electromagnetic torque [2].

Lorentz force eddy current testing (LET) is another newly introduced non-destructive testing (NDT) technique in this framework of MECT [3]. It is based on the relative, translational movement between a permanent magnet and a conductive, non-ferromagnetic material. The permanent magnet moves with constant velocity in a small lift-off distance above the object under test. Due to the relative movement eddy currents are induced in the conductor resulting in a Lorentz force exerting on the conductor and, according to Newton's third law, also on the magnet. Pertubations in the conductivity, e.g. caused by a defect in form of a crack, can be detected because of the resulting change in the profile of the Lorentz force.

In this paper, we present recent developments in LET: the magnet design is the most crucial element to improve the technique. Hence, we present the optimization of an innovative magnetic Halbach structure enhancing the Lorentz force. Furthermore, an uncertainty analysis of the used experimental setup is performed to identify the most significant sources

of variances. Finally, a detection limit is determined using a quasi-infinite crack in order for comparison with classical ECT.

2. Optimal Magnet Design

The performance of such a LET system can be enhanced by applying optimization schemes to determine magnet systems with high magnetic energy focusing the magnetic flux in the conductor. In LET the optimization goal is to maximize the response resulting from a defect surrounded by conductive material leading to an increasing signal-to-noise-ratio.

Because of the high variety of NDT problems the methodology has been developed as generally as possible in order to characterize and address the problem specificity [4]. In the optimization study we focus on non-magnetic, electrically conducting specimen assuming a smooth surface and a defect that is far away from any lateral boundaries to neglect edge effects. This scheme can be easily adapted to different geometries and has already be applied to small metal injection molding specimen [5].

The optimization was performed with respect to the maximum of the absolute defect response amplitude (ADRA) ΔF_x resulting from the difference between the perturbed drag-force of the conductor $F_x^{(d)}$ including the defect and the unpertubed drag-force $F_x^{(0)}$:

$$\Delta F_x = \max\left|F_x^{(d)} - F_x^{(0)}\right| \tag{1}$$

The geometric parameters of the problem and the ADRA are shown together in Figure 1. The conductor is modeled as pseudo-infinite half-space including a cuboidal defect with edge length a situated in a depth d.

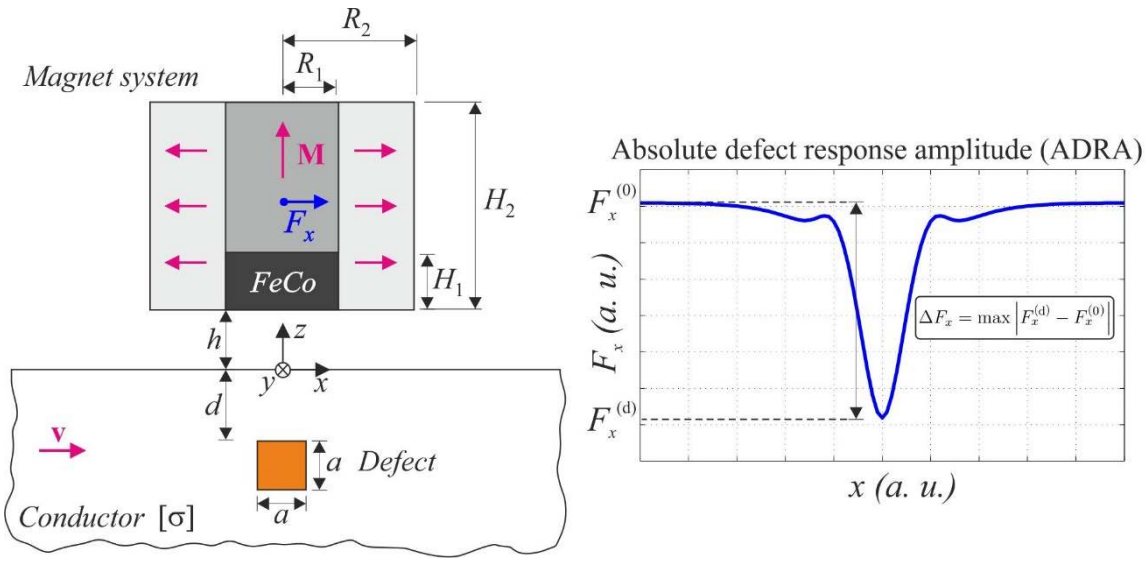

Fig. 1. Geometrical parameters of the LET setup, design variables of the magnet system and illustration of the absolute defect response amplitude used as objective function.

The conductivity tensor $[\sigma]$ enables also anisotropic conductivity properties of the conductor, e.g. laminated structures. The lift-off distance between the magnet and the conductor is given by the distance h. The specimen moves with a velocity $v = v_x$ relatively to the magnet.

The concept of focusing the magnetic field was developed by Mallinson [6] and Halbach [7] which we extended to a cylindrical structure. We investigated a cylindrical Halbach

structure consisting of an outer radial magnetized ring and an inner axial magnetized cylinder, both made of VACODYM® 745HR, a hard magnetic NdFeB-material with a nominal remanence of B_r = 1.44 T. Furthermore, the inner disc of height H_1 is made of soft magnetic iron-cobalt-alloy (VACOFLUX® 50) with a saturation polarization of 2.3 T which is provided by VACUUMSCHMELZE GmbH & Co. KG, Hanau, Germany.

This structure can be entirely geometrically described by the outer and inner radii R_2 and R_1, the height of the ferromagnetic disc H_1 and the height of the whole structure H_2. Three different magnet geometries are included in this design, the standard cylindrical permanent magnet (C), a cylindrical Halbach structure (HC) and a cylindrical Halbach structure supported by highly saturated soft magnetic material such as FeCo-alloys (HCp). In the general case, the dimensionless design variables **x** are defined as:

$$\mathbf{x} = \left[\frac{H_2}{R_2}, \frac{R_1}{R_2}, \frac{H_1}{H_2}\right]. \tag{2}$$

For C and HC systems, particular design variables become constant and the number of free variables is reduced.

In case of negligible secondary magnetic field, a scaling factor for the drag-force F_x can be defined

$$S = \sigma \, \mathrm{v} \, B_r^2 h^3 \, , \tag{3}$$

where the remanence B_r is only part of the scaling factor when no ferromagnetic material is used (C or HC systems). In case of HCp systems the non-linear $B(H)$-curve of the soft magnetic material has to be taken into account. The optimization is performed based on reference values. The obtained results have to be denormalized according to the scaling factor S of the specific problem of interest. The system investigated can now be fully described by a set of system parameters

$$\mathbf{p} = \left[\frac{V_\mathrm{m}}{V_\mathrm{d}}, \frac{d}{h}, \frac{a}{h}, \boldsymbol{a}_\sigma, B_r \, , B(H)\right], \tag{4}$$

where $\mathrm{V}_m = \pi \, R_2^2 H_2$ is the magnet volume and $\mathrm{V}_d = a^3$ is the volume of the equivalent cuboidal defect. The anisotropy vector $\boldsymbol{a}_\sigma$ describes the anisotropy of the specimen given by $[\sigma] = \sigma \, \mathrm{diag}(\boldsymbol{a}_\sigma^T)$ as in case of laboratory setup with aluminium sheets ($\boldsymbol{a}_\sigma = [1, 1, 0]^T$) preventing current flow between sheets in z-direction.

In order to determine the optimal design variables, a linear constraint reflecting the geometrical limits of the design variables has to be defined. Furthermore, in case of a maximum load for the force sensor, a non-linear inequality constraint has to be defined limiting the maximum drag-force in the unpertubed case. In our experimental setup the maximum load for the drag-force is limited to $F_x^{(0)}$ = 3 N. For the optimization the absolute defect response amplitude (ADRA) has to be maximized.

For the optimization procedure we used sequential quadratic programming (SQP). In the modeling using the finite element method (FEM) the secondary magnetic field generated by the induced eddy currents is neglected, i.e. the weak reaction approach [8]. We used the MATLAB® implementation *fmincon* to couple the FEM solver of COMSOL Multiphysics® and the SQP algorithm by means of the LiveLink™ for MATLAB®. More details of the optimization scheme can be found in [4].

Here, we present two different defect scenarios with anisotropic behaviour $\boldsymbol{a}_\sigma = [1, 1, 0]^T$, one for small subsurface defects and the other for medium sized deeper defects at a lift-off distance h = 1 mm, a velocity $v = 0.5\, m/s$ and a specimen conductivity of $\sigma = 30.66\ \mathrm{MS/m}$. In the optimization we compared the results of all three different magnet designs for both scenarios.

For small subsurface defects (V_m= 7000 mm³, d = 2 mm, a = 2 mm) a Halbach structure (Figure 2.a) section emerged as optimal magnet with optimal design variables $\mathbf{x}_{opt}$ = [1.17, 0.22, 0.54] (compare equation (2)). The HC and HCp structure generate defect responses of 28.1 mN and 32.4 mN which correspond to a gain up to ~180% and ~140 %, respectively, compared with the optimal cylinder fulfilling the force constraint $F_x^{(0)}$ = 3 N.

The spatial distribution of the magnetic flux density **B** and induced current density **J** are shown in Figure 2.a. The Halbach structure with iron-cobalt disc (HCp) is focusing the magnetic flux and hence, the induced eddy current density under the inner part of the magnet system increased, resulting in much stronger defect response.

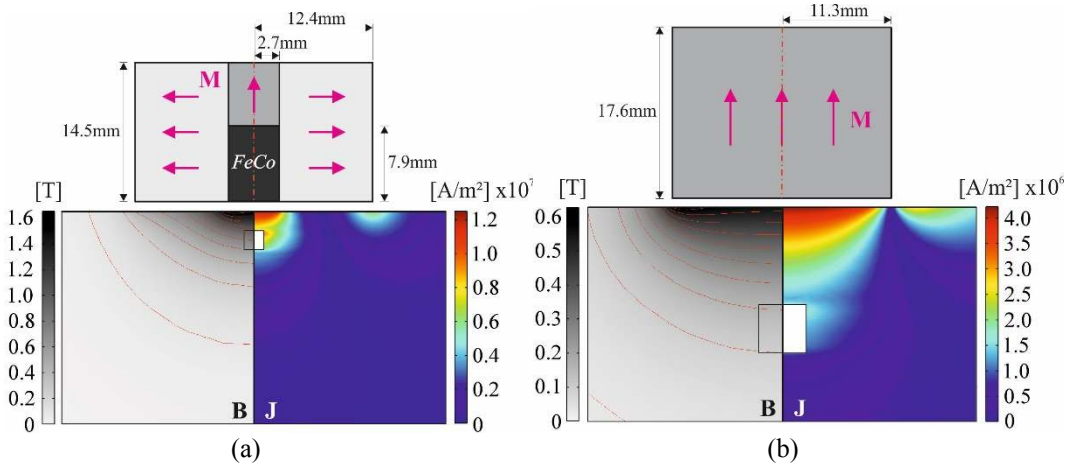

Fig. 2. Magnitude of flux density **B** and induced eddy current density **J** optimized for anisotropic specimens. Cross sections of optimized magnet structures for (a) a Halbach-cylinder with iron-cobalt (small subsurface defect) and (b) a cylindrical magnet (deep medium sized defect)

For deep medium sized deep defects (V_m= 7000 mm³, d = 10 mm, a = 5 mm) the optimization procedure leads to an optimal magnet in shape of a cylindrical magnet (C) with $\mathbf{x}_{opt}$ = [1.56, 1, 0] in a similiar way as for the Halbach structure (HCp) (Figure 2.b).

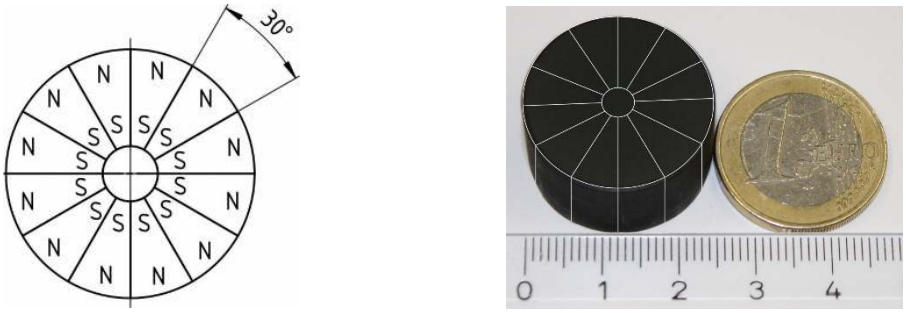

Fig 3. Top view of Halbach magnet made by VACUUMSCHMELZE GmbH & Co. KG, Hanau, Germany as engineering drawing (left) and final magnet in comparison to Euro coin (right)

The optimized Halbach structure (HCp) enhances the defect responses for subsurface defects focusing the eddy currents and leads to a higher magnetic flux density of 1.6 T compared to 0.6 T on the surface of the conductor in case of a cylindrical magnet (Figures 2.a and 2.b).

Figure 3 on the left shows the top view on the Halbach magnet as it was planned consisting of 12 segments (30° degrees). On the right hand side in Figure 3 the produced Halbach magnet is shown made of VACODYM® 745HR as hard magnetic NdFeB-material and soft magnetic iron-cobalt-alloy (VACOFLUX® 50) by VACUUMSCHMELZE GmbH & Co. KG, Hanau, Germany.

The proposed optimization scheme was implemented in a modular way and therefore can be easily adopted to different geometries, like in case of the small metal injection molding specimen where the edge effects could not be neglected.

3. Analysis of Uncertainty

Numerical simulation as used in the described optimization scheme enables the prediction of Lorentz force profiles, but it does not take into account the intrinsic variability of the input parameters used in the numerical model. The identification of the main sources of uncertainty can help to improve the experimental setup. Therefore, we applied a non-intrusive generalized polynomial chaos (gPC) expansion to quantify the impact of multiple unknown input parameters influencing the Lorentz force. For the gPC expansion the probability density functions (PDFs) of the interesting parameters are determined by measuring or an estimation in case no measurement is possible. Hence, in contrast to the many evaluations needed in Monte Carlo method the gPC expansion needs only quite a small number of evaluations of the numerical model to determine the PDF of the output (including statistical parameters as mean and variance). As a result of the gPC expansion, the main influencing parameters on the output function can be determined by the analysis of variance in form of Sobol decomposition [9].

In the context of LET, the variability of the lift-off distance h, conductivity σ, the velocity v and the remanence B_r have to be considered. The lift-off distance h was estimated by the accuracy of the used 2D-linear stage. The statistical properties of the other three parameters were determined experimentally. The conductivity σ of the used aluminium sheets was measured with an eddy current testing device. The velocity variations were determined by the differentiation of the data of approximately 19,000 samples collected by the incremental position decoder used in our laboratory setup. Finally, the remanence of 100 cylindrical magnets from one supplier made of NdFeB-material with a material grade N52 was measured using a Hall sensor.

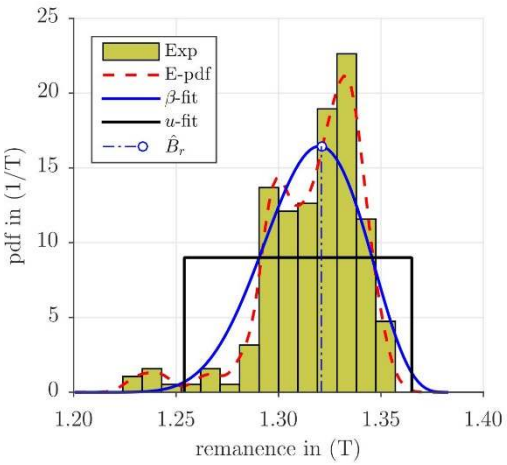

Fig. 4: Statistical properties of the input parameter magnetic remanence. The graph shows the histogram (Exp), the associated empirical PDF (E-pdf) and the fitted distributions used in the simulations.

As an example for the PDF of an input parameter, the measured remanence B_r as histogram and the fitted uniform and β-distributions are shown in Figure 4. Both types of PDFs as fits for the input parameters demand different types of polynomials for the gPC expansion. The results gained by the gPC in only a few simulations were compared to results of Monte Carlo method with 10,000 runs and showed good agreement (error below 0.37%). Using the Sobol decomposition, the determined first order Sobol indices are most significant and cover almost the total variance (Table 1). By means of the gPC expansion, treating the numerical model of LET as a black box, it turned out

that the uncertainty of magnetic remanence has the greatest influence (~85%) followed by the lift-off distance, contributing approximately ~10% to the total uncertainty of the Lorentz force. The remaining two parameters have only a minor influence on the uncertainty of the Lorentz force.

Table 1: First order Sobol coefficients of F_x and F_z averaged over $M = 11$ magnet positions with a grid of $q = 3$ in each direction and expansion order of $p = 3$

PDF	$S_{x,B}^{(1)}$	$S_{z,B}^{(1)}$	$S_{x,h}^{(1)}$	$S_{z,h}^{(1)}$	$S_{x,v}^{(1)}$	$S_{z,v}^{(1)}$	$S_{x,\sigma}^{(1)}$	$S_{z,\sigma}^{(1)}$
uni	88.4	84.2	9.6	10.2	1.3	3.7	0.7	1.9
beta	87.9	83.7	10.2	10.7	1.2	3.6	0.7	2.0

Furthermore, it could be observed that the remanence of the magnets is lower than expected from the manufacturer's information for material grade N52 (B_r = 1.43 T compared to our mean value of 1.32 T). Finally, a measurement was performed and it was compared to a simulation of the estimated force profiles showing good agreement in the range of the variances determined by the uncertainty analysis. More details about the uncertainty analysis can be found in [9].

4. Defect Depth Study

Previous ECT studies often assumed quasi-infinite cracks to evaluate the detection limit. In this case, the defect is a slit in the specimen under test with a length chosen in relation to the sensor system. In order to ensure comparability to the reports in the literature, a benchmark problem is defined. The geometry is inspired by a study from Mook et al. [10] and shown in Figure 5.

The specimen consists of a solid block of size [250,50,24] mm made of aluminium, containing a long slit of size $[X_d, Y_d, Z_d] = [75, 1.5, 24]$ mm. The slit is oriented parallel to the direction of motion in order to provide highest possible eddy current perturbation.

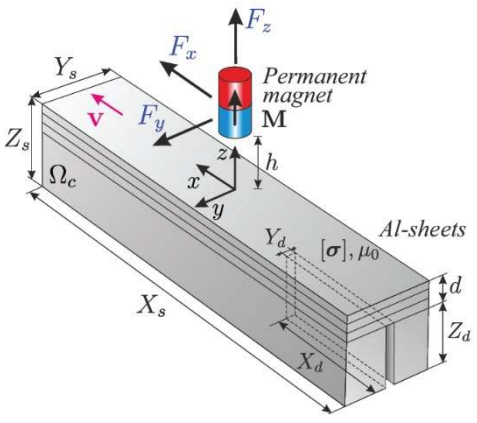

Fig. 5: Geometry of the geometrical setup to detect a deep lying slit defect

On top of this structure a variable number of aluminium sheets with thickness $t = 2$ mm is put on the top of each other. Hence, this enables to vary the defect depth d from 0 to 36 mm using 18 sheets. The sheets which are not put on the top of the specimen are situated on the bottom of the structure in order to ensure a constant height the assembled specimen. The outer dimensions of the problem are not altered and the magnetic Reynolds number is also kept constant. The overall dimensions of the whole assembly are $[X_S, Y_S, Z_S] = [250, 50, 60]$ mm. A cylindrical magnet of size $[D_m, H_m] = [22.5, 17.6]$ mm of grade N52 was moved with a constant velocity of $v = 0.5$ m/s at a lift-off distance $h = 1$ mm. For all aluminium sheets their conductivity was experimentally determined (mean value $\bar{\sigma}_{Sheets} = 30.60$ MS/m) and also for the specimen block ($\sigma_B = 25.75$ MS/m).

During the post-processing, the measured data is aligned and averaged over the 20 repetitions. Furthermore, it is filtered with a 10th order Butterworth low-pass filter with cut-

off frequency of 100 Hz. The force profiles are normalized with respect to the stationary values in the unpertubed case. The normalization provides comparability between the different measurements due to the conductivity variations between block and sheets.

The results of the normalized drag- and lift force over the whole specimen are shown in Figure 6.a and 6.b, respectively. The area, where the slit is located, is shown on the right hand side in magnified form.

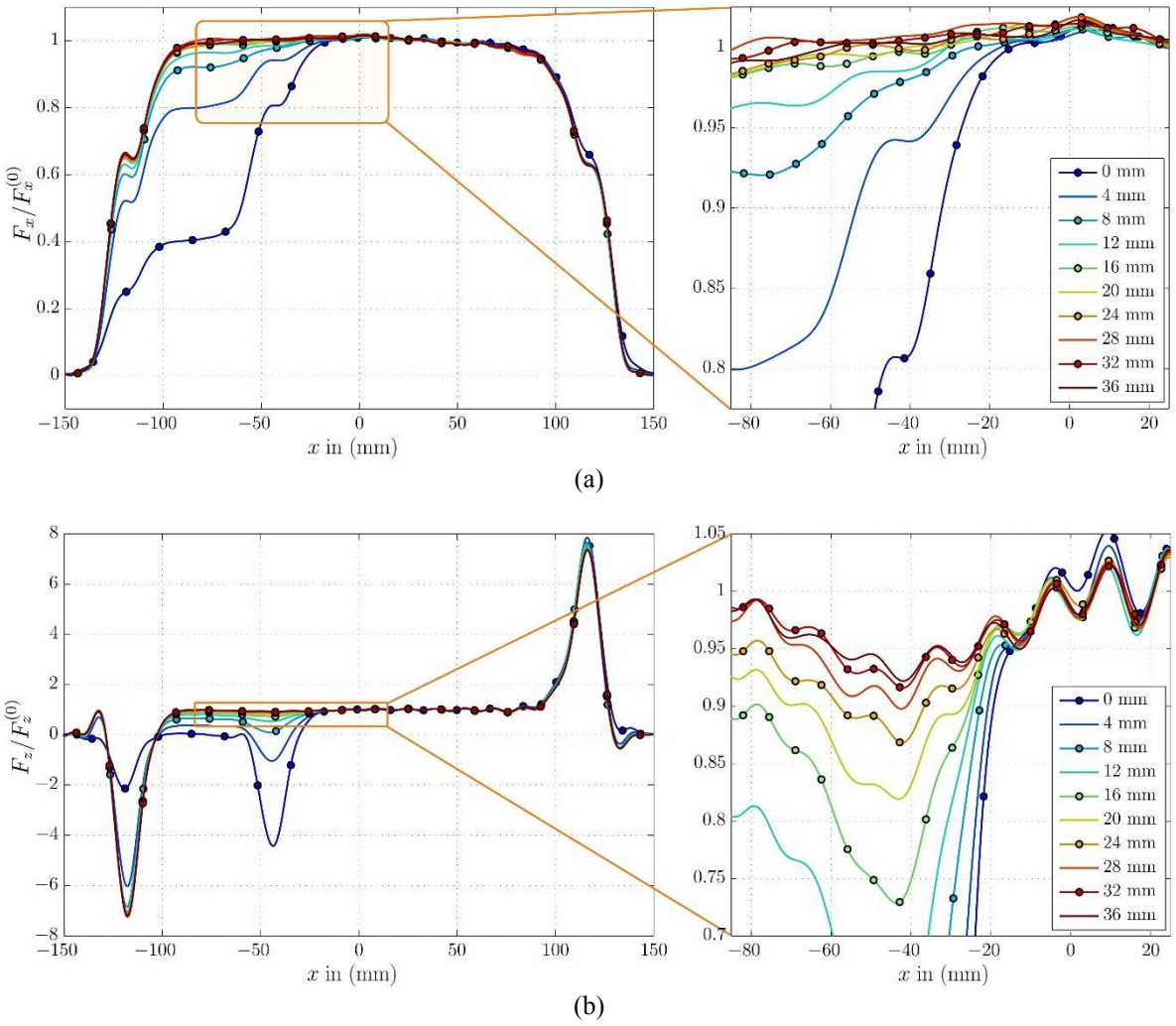

Fig. 6: Measured profiles of the drag-force (a) and lift-force (b) during the investigation on the maximum defect depth. The specimen contains a slit of size $[X_d, Y_d, Z_d] = [75, 1.5, 24]$ mm, which is located at different depths.

Based on the definition of the velocity of the specimen, the data is recorded over time from right to the left such that positive x-positions are sampled first in time. When the specimen approaches the magnet and comes close to the magnet, the drag-force ramps up and the lift-force shows a characteristic peak before both components reach their steady state ($F_x^{(0)}$ and $F_z^{(0)}$).

In the defect region, the pertubations of both components of the Lorentz force are analyzed. In case of the drag-force, pertubations due to the slit can be recognized up to a defect depth $d = 12$ mm. In contrast, when the lift-force is considered, the slit can be clearly observed up to a defect depth of $d = 24$ mm.

Especially in the lift component of the force parasitic oscillations can be seen. These are systematic effects which are partially produced by the measurement frame of the laboratory setup. If the parasitic disturbances in the forces components can be reduced, the detectable defect depth will increase.

With the help of this analysis, LET can now be classified in the framework of electromagnetic eddy current methods in a qualitative sense. Compared with the results presented in [10], Lorentz force eddy current testing with its present realization is comparable concerning the achievable defect depth detection limit. However, it has to be pointed out that in contrast to normal eddy current testing methods in LET the object is in motion and is tested contactless within a few seconds, which is a decisive difference to traditional ECT methods.

5. Conclusions

In this paper, we presented recent advancements in Lorentz force eddy current testing as a method of motion induced eddy current testing (MECT). The proposed optimization approach to determine an optimal magnet design leads to a new cylindrical Halbach structure enhancing the Lorentz force especially for subsurface defect scenarios. Furthermore, the uncertainty of our laboratory setup was calculated and compared with experimental results showing good agreement. Finally, a defect detection limit based on a quasi-infinite crack was determined and showed the compatibility of this newly introduced non-destructing testing technique compared to classical ECT studies.

References

[1] H. M. G. Ramos, T. Rocha, D. Pasadas, and A. Ribeiro, "Velocity induced eddy currents technique to inspect cracks in moving conducting media," Proceedings of the International Instrumentation and Measurement Technology Conference (I2MTC), pp. 931–934, 2013.

[2] Y. Tan, X. Wang, and R. Moreau, "An innovative contactless method for detecting defects in electrical conductors by measuring a change in electromagnetic torque," Measurement Science and Technology, vol. 26, no. 3, p. 035 602, 2015.

[3] H. Brauer, K. Porzig, J. Mengelkamp, M. Carlstedt, M. Ziolkowski, and H. Toepfer, "Lorentz force eddy current testing: a novel NDE-technique," COMPEL, vol. 33, no. 6, pp. 1965–1977, 2014.

[4] K. Weise, R. Schmidt, M. Carlstedt, M. Ziolkowski, H. Brauer, and H. Toepfer, "Optimal Magnet Design for Lorentz Force Eddy Current Testing," IEEE Transactions on Magnetics, vol. 51, no. 9, 6 201 415, 2015.

[5] R. Schmidt, K. Weise, M. Carlstedt, M. Ziolkowski, H. Brauer, and H. Toepfer, "Optimized Lorentz Force Eddy Current Testing for Small Metal Injection Molding Specimens", in: 20th International Workshop on Electromagnetic Nondestructive Evaluation (ENDE), Sendai, Japan 2015.

[6] J. C. Mallinson, "One-sided fluxes – A magnetic curiosity?" IEEE Transactions on Magnetics, vol. 9, no. 4, pp. 678–682, 1973.

[7] K. Halbach, "Design of Permanent Multipole Magnets with Oriented Rare-Earth Cobalt Material," Nuclear Instrumentation & Methods, vol. 169, no. 1, pp. 1–10, 1980.

[8] M. Zec, R. P. Uhlig, M. Ziolkowski, and H. Brauer, "Fast Technique for Lorentz Force Calculations in Nondestructive Testing Applications," IEEE Transactions on Magnetics, vol. 50, no. 2, 7 003 104, 2014.

[9] K. Weise, M. Carlstedt, M. Ziolkowski, and H. Brauer, "Uncertainty Analysis in Lorentz Force Eddy Current Testing," IEEE Transactions on Magnetics, vol. 52, no. 3, 6 200 104, 2016.

[10] G. Mook, O. Hesse, and V. Uchanin, "Deep Penetrating Eddy Currents and Probes," Proceeding of the ECNDT, 2006.